Tunable Magnon Weyl Points in Ferromagnetic Pyrochlores

Alexander Mook,[1] Jürgen Henk,[2] and Ingrid Mertig[1,2]
[1]Max-Planck-Institut für Mikrostrukturphysik, D-06120 Halle (Saale), Germany
[2]Institut für Physik, Martin-Luther-Universität Halle-Wittenberg, D-06099 Halle (Saale), Germany
(Received 25 June 2016; revised manuscript received 17 August 2016; published 7 October 2016)

The dispersion relations of magnons in ferromagnetic pyrochlores with Dzyaloshinskii-Moriya interaction are shown to possess Weyl points, i. e., pairs of topologically nontrivial crossings of two magnon branches with opposite topological charge. As a consequence of their topological nature, their projections onto a surface are connected by magnon arcs, thereby resembling closely Fermi arcs of electronic Weyl semimetals. On top of this, the positions of the Weyl points in reciprocal space can be tuned widely by an external magnetic field: rotated within the surface plane, the Weyl points and magnon arcs are rotated as well; tilting the magnetic field out of plane shifts the Weyl points toward the center $\bar{\Gamma}$ of the surface Brillouin zone. The theory is valid for the class of ferromagnetic pyrochlores, i. e., three-dimensional extensions of topological magnon insulators on kagome lattices. In this Letter, we focus on the (111) surface, identify candidates of established ferromagnetic pyrochlores which apply to the considered spin model, and suggest experiments for the detection of the topological features.

DOI: 10.1103/PhysRevLett.117.157204

Introduction.—Ferromagnetic pyrochlores attracted attention with the experimental discovery of the magnon Hall effect [1]. This transverse transport is explained by a Berry curvature [2–4] which is introduced by the Dzyaloshinskii-Moriya (DM) interaction [5,6]. In addition, the Chern numbers of magnon bulk bands are nonzero, and in accordance with the bulk-boundary correspondence [7,8] topological magnons are found at the edges of two-dimensional kagome lattices [9,10]. Hence, systems featuring topological magnon states are dubbed "topological magnon insulators" (TMIs) [9], because they exhibit many features of electronic topological insulators [11].

In this Letter, we predict that ferromagnetic pyrochlores exhibit features of another important class of topologically nontrivial systems, namely electronic Weyl semimetals [12,13]. Their magnon dispersion relations possess a pair of Weyl points on a line in reciprocal space which is along an external magnetic field; the Weyl points possess opposite topological charges of ± 1.

At a surface, magnon surface states connect the surface-projected Weyl points; since the associated constant-energy cuts are open they are analogs of Fermi arcs in electronic Weyl semimetals. These arcs turn out to be tunable: upon rotating the magnetic field within the surface plane they follow the likewise rotated Weyl points. An out-of-plane rotation reduces the length of the arcs until they collapse at the center $\bar{\Gamma}$ of the surface Brillouin zone (when the field is perpendicular to the surface), a feature calling for experimental verification.

We recall that recently magnon Weyl points have been predicted in breathing pyrochlore lattices with spin anisotropy and a noncollinear ground state [14]. However, the present model relies on a ferromagnetic ground state and on the DM interaction; it is thus a natural extension of TMIs on kagome lattices [9,10] to three dimensions.

Model and spin-wave analysis.—The pyrochlore lattice is a face-centered cubic (fcc) lattice of corner-sharing tetrahedra, with four atoms in its basis [Fig. 1(a)]. Lacking inversion symmetry with respect to the midpoints of bonds, it features DM interactions. Moriya's symmetry rules [6] indicate that the DM vectors $\boldsymbol{D}_{ij}$ are perpendicular to the bond that links site i with site j; they are situated at the faces of cubes that enclose tetrahedra [Fig. 1(b)] [1,15,16].

The minimal magnetic Hamiltonian which includes isotropic symmetric exchange J_{ij}, DM interactions $\boldsymbol{D}_{ij}$, and a Zeeman term with external magnetic field $\boldsymbol{B}$ reads

$$H = -\sum_{ij} J_{ij}\boldsymbol{s}_i \cdot \boldsymbol{s}_j + \sum_{ij} \boldsymbol{D}_{ij} \cdot (\boldsymbol{s}_i \times \boldsymbol{s}_j) - \sum_i \boldsymbol{B} \cdot \boldsymbol{s}_i, \qquad (1)$$

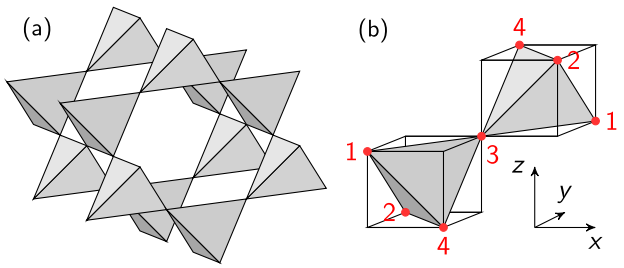

FIG. 1. Pyrochlore lattice. (a) Part of the crystal structure. (b) Four basis sites (1–4) with the nearest-neighbor DM vectors given by $\boldsymbol{D}_{12} = D/\sqrt{2}(0,-1,-1)$, $\boldsymbol{D}_{13} = D/\sqrt{2}(-1,1,0)$, $\boldsymbol{D}_{14} = D/\sqrt{2}(1,0,1)$, $\boldsymbol{D}_{23} = D/\sqrt{2}(1,0,-1)$, $\boldsymbol{D}_{24} = D/\sqrt{2}(-1,-1,0)$, and $\boldsymbol{D}_{43} = D/\sqrt{2}(0,-1,1)$.

where $\boldsymbol{s}_i$ is the spin operator at site i. For $J_{ij} > 0$ the ferromagnetic state is the ground state with order parameter $\boldsymbol{n} = \boldsymbol{B}/B$; the collinearity is stable against the DM interaction [1]. In the following, the (tiny) rigid energy shift due to the Zeeman energy is neglected and only $\boldsymbol{n}$ is kept for simplicity, that is, the limit $B \to 0^+$ is considered.

As argued in Ref. [1], only the component of $\boldsymbol{D}_{ij}$ parallel to $\boldsymbol{n}$ contributes to the linear spin-wave Hamiltonian. The spin-wave approximation is performed in an orthonormal basis $\{\boldsymbol{l}, \boldsymbol{m}, \boldsymbol{n}\}$, where ladder operators $s_i^{\pm} = s_i^l \pm \mathrm{i} s_i^m$ are introduced. After an adequate Holstein-Primakoff [17] transformation, a Fourier transformation of the boson operators yields the 4×4 spin-wave Hamilton matrix $H_{\boldsymbol{k}}$. Allowing for nearest-neighbor interactions with strength J_{N} as well as next-nearest-neighbor interactions with strength J_{NN}, the matrix elements read $H_{\boldsymbol{k},\mu\mu} = 6s(J_{\mathrm{N}} + J_{\mathrm{NN}})$, and $H_{\boldsymbol{k},\mu\nu} = -2s(J_{\mathrm{N}} + \mathrm{i}D^{\boldsymbol{n}}_{\mu\nu}) \cos(\boldsymbol{k} \cdot \boldsymbol{\delta}^{\mathrm{N}}_{\mu\nu}) - 2sJ_{\mathrm{NN}} \cos(\boldsymbol{k} \cdot \boldsymbol{\delta}^{\mathrm{NN}}_{\mu\nu})$ for $\mu \neq \nu$; here, $D^{\boldsymbol{n}}_{\mu\nu} \equiv \boldsymbol{D}_{\mu\nu} \cdot \boldsymbol{n}$ and $\boldsymbol{\delta}^{\mathrm{N}}_{\mu\nu}$ ($\boldsymbol{\delta}^{\mathrm{NN}}_{\mu\nu}$) connects nearest (next-nearest) basis sites μ and ν ($\mu, \nu = 1, 2, 3, 4$). To mimic pyrochlore systems, we set $s = 1/2$ for all basis sites.

We now analyze magnon spectra $\varepsilon_{\nu\boldsymbol{k}}$ and Berry curvatures [3,4,9,18–20]

$$\Omega_{\nu\boldsymbol{k}} \equiv \mathrm{i} \sum_{\mu \neq \nu} \frac{\langle \boldsymbol{u}_{\nu\boldsymbol{k}} | \partial_{\boldsymbol{k}} H_{\boldsymbol{k}} | \boldsymbol{u}_{\mu\boldsymbol{k}} \rangle \times \langle \boldsymbol{u}_{\mu\boldsymbol{k}} | \partial_{\boldsymbol{k}} H_{\boldsymbol{k}} | \boldsymbol{u}_{\nu\boldsymbol{k}} \rangle}{(\varepsilon_{\nu\boldsymbol{k}} - \varepsilon_{\mu\boldsymbol{k}})^2}, \quad (2)$$

where $|\boldsymbol{u}_{\nu\boldsymbol{k}}\rangle$ is an eigenvector of $H_{\boldsymbol{k}}$ with energy $\varepsilon_{\nu\boldsymbol{k}}$. $\Omega_{\nu\boldsymbol{k}}$ encodes the nontrivial topology of the bulk bands which is related to global symmetries: inversion symmetry $\mathcal{I}$ (time-reversal symmetry $\mathcal{T}$) causes $\Omega_{\nu\boldsymbol{k}}$ to be even (odd) in $\boldsymbol{k}$.

Typical results are summarized in Figs. 2(a)–(d). (a) For $J_{\mathrm{NN}} = 0$ and $D = 0$, the four magnon bands are not gapped, the third and fourth band are dispersionless and degenerate. $\Omega_{\nu\boldsymbol{k}}$ vanishes in the entire Brillouin zone (BZ) since $\mathcal{I}$ and $\mathcal{T}$ are conserved. The direction $\boldsymbol{n}$ of the magnetic field does not affect the spectrum. (b) $\mathcal{T}$ is broken for $D > 0$, the upper two magnon branches become dispersive, and $\Omega_{\nu\boldsymbol{k}}$ is nonzero for all bands. The band structure depends sensitively on $\boldsymbol{n}$. As long as $\boldsymbol{n}$ is *not* within a $\{100\}$ plane, a tiny fundamental gap between the first and second band shows up (inset). More strikingly, on any line in reciprocal space through the origin Γ and parallel to $\boldsymbol{n}$, the second and the third band cross each other at two $\boldsymbol{k}$. These $\boldsymbol{k}$ lie symmetrically to Γ, their spacing is determined by $\boldsymbol{n}$ and $|D|$. As we will show, these band crossings are *Weyl points* [red circle; cf. Fig. 3(a)]. (c) The Weyl points are robust against $J_{\mathrm{NN}} \neq 0$ (inset) as $\mathcal{I}$ remains preserved. For antiferromagnetic J_{NN} ($J_{\mathrm{NN}} < 0$, small enough to retain the ferromagentic ground state), the Weyl points are located in energy so that no other bulk band has the same energy (for any $\boldsymbol{n}$), that is, they are type-I Weyl points [21]. (d) The Weyl cones are tilted upon varying $\boldsymbol{n}$ or J_{NN}. In particular type-II Weyl points [21] can occur for $J_{\mathrm{NN}} > 0$.

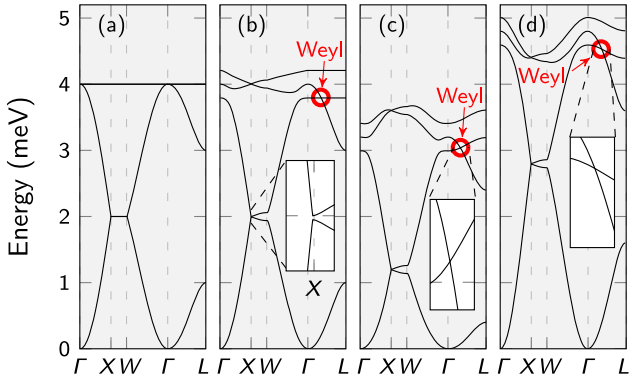

FIG. 2. Magnon spectrum of ferromagnetic pyrochlores for $J_{\mathrm{N}} = 1$ meV and (a) $J_{\mathrm{NN}} = D = 0$, (b) $J_{\mathrm{NN}} = 0$, $D = 0.28$ meV, (c) $J_{\mathrm{NN}} = -0.1$ meV, $D = 0.28$ meV, and (d) $J_{\mathrm{NN}} = +0.1$ meV, $D = 0.28$ meV. The magnetic field points along $\boldsymbol{n} = (1,1,1)/\sqrt{3}$, i. e., along $\Gamma \to L$. Red circles in (b), (c), and (d) mark Weyl points. See Fig. 3(a) for the high-symmetry points of the fcc BZ.

Topology of bulk bands.—The nontrivial topology is brought about by the DM interaction, as is evident from expanding Eq. (1) in terms of small deviations $\boldsymbol{\delta}$ from the ferromagnetic ground state (the following arguments are in line with Refs. [1,2,22,23]). Without loss of generality, we take $\boldsymbol{n} = \hat{\boldsymbol{z}}$ and $\boldsymbol{s}_i = \hat{\boldsymbol{z}} + \boldsymbol{\delta}_i$. Neglecting for the moment prefactors, a constant, and the Zeeman energy, the deviations yield $\delta H = \delta H_{\mathrm{ex}} + \delta H_{\mathrm{DM}}$, with $\delta H_{\mathrm{ex}} = -\sum_{ij} J_{ij}(\delta_i^z + \delta_j^z + \boldsymbol{\delta}_i \cdot \boldsymbol{\delta}_j)$ and $\delta H_{\mathrm{DM}} = \sum_{ij} D_{ij}(\delta_i^x \delta_j^y - \delta_i^y \delta_j^x)$. Terms in first order in $\boldsymbol{\delta}_i$ in δH_{DM} cancel because $\sum_j \boldsymbol{D}_{ij} = 0$.

The inversion $\mathcal{I}$ interchanges $i \leftrightarrow j$, it is obeyed by both δH_{ex} and δH_{DM} (note that $D_{ij} = -D_{ji}$). δH_{ex} also obeys the pseudotime-reversal $\mathcal{T}$ which is a spin flip $\boldsymbol{\delta}_i \to -\boldsymbol{\delta}_i$ followed by a rotation in spin space by π about an axis perpendicular to $\hat{\boldsymbol{z}}$. However, this does *not* apply to δH_{DM}.

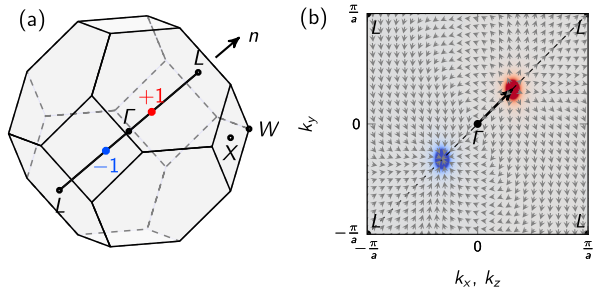

FIG. 3. Weyl points and Berry curvature. (a) Fcc BZ with high-symmetry points, field direction $\boldsymbol{n}$, and Weyl points (dots). (b) Normalized dipole vector field $\Omega_{2\boldsymbol{k}}$ of band 2 in the $k_x = k_z$ plane, with Γ and L points indicated. The color scale depicts the divergence of the vector field (blue: negative; gray: zero; red: positive); the two Weyl points appear in the center of the blue and red spot, respectively. Parameters as in Fig. 2(c), $\boldsymbol{n} = (1,1,1)/\sqrt{3}$, i. e., along $\Gamma \to L$ (indicated by the black arrow).

With $\mathcal{I}$ preserved and $\mathcal{T}$ broken, a single pair of Weyl points is allowed [24]. As $\mathcal{I}$ implies $\varepsilon_\nu(\boldsymbol{k}) = \varepsilon_\nu(-\boldsymbol{k})$ the two Weyl points appear at the same energy.

The above mechanism is at variance with that predicted in Ref. [14]. There, the nontrivial topology is brought about by a local spin anisotropy, and the resulting complicated ground state allows for more than two Weyl points.

In the remainder of this Letter, we present results obtained for the exchange parameters of Fig. 2(c), i. e., for type-I Weyl points.

An integer Chern number $C_\nu = (1/2\pi)\int_S \Omega_{\nu\boldsymbol{k}} \cdot \tilde{\boldsymbol{n}} dS$ is calculated for each band ν; S is a closed and oriented surface in the bulk BZ with surface normal $\tilde{\boldsymbol{n}}$. Letting $\tilde{\boldsymbol{n}} = \text{const.}$, S is a 2D slice of the 3D BZ. By moving the slice in the BZ, $C_\nu(\lambda)$ can be calculated as a function of the position λ of the slice [25].

$C_1(\lambda) = -\text{sgn}(D)$ is constant (here, $\tilde{\boldsymbol{n}} = \boldsymbol{n}$) because a fundamental band gap separates the lowest from the other bands [inset in Fig. 2(b)]. $C_2(\lambda)$ and $C_3(\lambda)$ are not globally but piece-wise constant because these bands touch each other at the Weyl points. The latter are monopoles of the Berry curvature vector field. To prove that the band crossings are Weyl points we show the Berry curvature vector field of band 2 [Fig. 3(b)]. There are two monopoles that appear as source (red spot, offset from Γ in the direction of the magnetic field) and sink (blue spot) of the vector field, providing evidence that the Weyl points have opposite topological charge q_2^{top}. Numerical integration yields $q_2^{\text{top}} = +1$ for the "red" (source) and $q_2^{\text{top}} = -1$ for the "blue" (sink) Weyl point [26].

Recapitulating, we have identified Weyl points in the bulk band structure of pyrochlore systems whose positions in reciprocal space and cone tilting can be tuned by an external magnetic field. A prominent feature of electronic Weyl semimetals are Fermi arcs which are surface states that connect projections of Weyl points onto the surface BZ. We now show that pyrochlore systems exhibit the magnon analogs of the (electronic) Fermi arcs, that is magnon arcs.

Surface states.—The surface magnon dispersion is analyzed in terms of the spectral density for semi-infinite systems which is calculated by Green function renormalization [27]. We exemplarily study the (111) surface and choose a quite large DM interaction ($D/J_N = 0.5$) to provide a clear picture. We would like to stress that the discussion is qualitatively valid for all surfaces and all D.

The (111) surface of the pyrochlore lattice is a kagome lattice; the resulting surface BZ is a hexagon [Fig. 4(a)]. Note that a magnetic field with an in-plane component breaks the rotational symmetry of the surface BZ. The magnetic field is completely in plane along $[11\bar{2}]$; hence, the projections of the Weyl points are situated on the line $\bar{M}' - \bar{\Gamma} - \bar{M}'$ [Fig. 4(b)].

The bulk bands appear as broad features in (b). The gaps between band 1 and 2 as well as band 2 and 3 are bridged by two topological surface states, TSS(1) and TSS(2). The latter obey the bulk-boundary correspondence [7,8,10,28].

Since the Chern number of band 1 equals -1, the winding number of the gap between band 1 and 2 equals -1 as well (the winding number is the sum of all Chern numbers of the bands below the considered gap). As the winding number dictates the number of topological surface states, there has to be one topological surface state: TSS(1). The bulk-boundary correspondence also holds for TSS(2), since the Weyl points carry topological charges (Chern numbers).

To show that TSS(1) and TSS(2) differ qualitatively, we present constant-energy cuts of the surface spectrum that cover the band gaps in which TSS(1) and TSS(2) are situated [(a) and (c)]. Both surface states are easily identified as bright lines clinging to the extended bulk features.

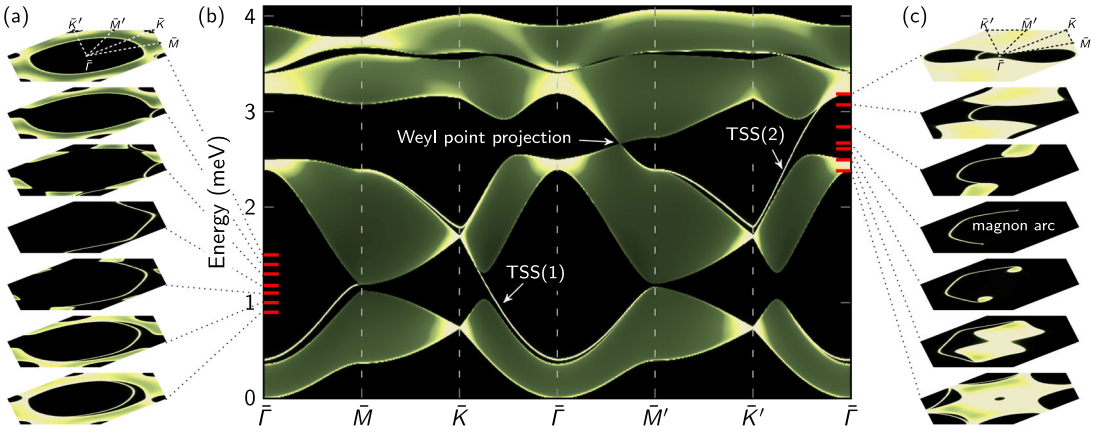

FIG. 4. Magnons at the (111) surface of a ferromagnetic pyrochlore. The surface spectral density is shown as color scale (black: zero; white: maximum). Bulk magnons appear as broad features, surface states as sharp lines. (a) and (c) show constant-energy cuts through the entire surface Brillouin zone for energies indicated by red lines in (b). (b) Spectral density along high-symmetry directions of the surface Brillouin zone. The projection of the Weyl points and two topological surface states (TSS) are indicated. Parameters as for Fig. 2(c), except $D = 0.5$ meV.

At $\varepsilon = 1.18$ meV bulk states do not contribute to the surface spectral density and only TSS(1) is visible [central cut in (a)]. Apparently, TSS(1) forms a closed line when considering the periodicity of the surface BZ.

Considering TSS(2), a similar scenario takes place at the energy of the Weyl points [$\varepsilon = 2.67$ meV, central cut of (c)]. Instead of a closed line, we find a *magnon arc* that connects the projections of the two Weyl points of opposite topological charge. Thus, pyrochlore ferromagnets host the magnon pendant to the Fermi arcs in electronic Weyl semimetals.

The Weyl points and the associated magnon arcs can be shifted—or tuned—by the magnetic field $\boldsymbol{B}$. The energy of the Weyl points is not affected by the rotation of $\boldsymbol{B}$; hence, all of the constant-energy contours discussed in what follows are at the same energy (2.67 meV).

By rotating the field within the surface plane [Fig. 5(a)], the Weyl points follow the magnetic field and can be rotated arbitrarily. Consequently, the magnon arc trails the Weyl point projections and is rotated likewise [(b)–(e)]. The arc is not rotated rigidly: it shows the largest distances from $\bar{\Gamma}$ along $\bar{\Gamma} - \bar{M}$ as well as $\bar{\Gamma} - \bar{M}'$ directions, irrespective of the magnetic field's azimuth. A sign change of either D or $\boldsymbol{n}$ would change the signs of the Berry curvature and of the topological charges; the magnon arc would be reflected about the direction of the magnetic field.

Rotating the magnetic field from in-plane to out-of-plane (bottom row in Fig. 5), the Weyl point projections are shifted toward $\bar{\Gamma}$, thereby reducing the length of the magnon arc. The arc "collapses" when the magnetic field points along the surface normal [Fig. 5(j)].

Experimental considerations.—The pyrochlore oxides $Lu_2V_2O_7$, $In_2Mn_2O_7$, and $Ho_2V_2O_7$, all of which exhibit the magnon Hall effect [29], are the most promising candidates for experimental detection of magnon Weyl points. The first two are modeled very well by the Hamiltonian in Eq. (1). For $Lu_2V_2O_7$, the ratio D/J_N of DM interaction to exchange interaction has been determined recently, with values of 0.32 [1], 0.18 [30], 0.07 [31], and 0.05 [32]. Since the DM interaction determines the distance between the Weyl points and Γ in reciprocal space, a search for Weyl points can help to identify the exact ratio. The tunability of the Weyl points and magnon arcs can be exploited, for example, in inelastic neutron scattering experiments [30]: the shifts of the bulk band crossings upon variation of the external magnetic field can be traced. By probing a fixed line in reciprocal space through the origin, say $\boldsymbol{q}$, one will see a band gap closing and reopening at one point on $\boldsymbol{q}$ upon evolution of the field's azimuth. The closing, i. e., the occurrence of Weyl points, coincides with the alignment of the field and $\boldsymbol{q}$.

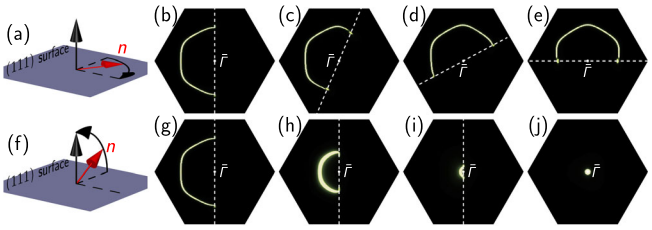

FIG. 5. Tuning magnon arcs in a pyrochlore ferromagnet by an external magnetic field. Top row (a)–(e): effect of rotating the magnetic field ($\boldsymbol{n}$, red) within the (111) surface (blue), as sketched in (a), on the magnon arc (b)–(e). Bottom row (f)–(j): as the top panels but for rotating $\boldsymbol{n}$ out of plane, as sketched in (f). In (j) the field is perpendicular to the surface and the magnon arc "collapses." The direction of $\boldsymbol{n}$ projected onto the (111) surface is indicated by white dashed lines. Parameters as for Fig. 4, except $\boldsymbol{n}$ which is varied.

Electron energy loss spectroscopy, which is sensitive to the surface [33], could be applied for the detection of the magnon arcs. Upon inversion of the magnetic field a magnon arc is reflected, whereas the surface spectral density of the bulk states is not. Hence, subtracting spectra of oppositely magnetized samples yields clear evidence of topological surface states.

Since the transverse thermal conductivities of $Lu_2V_2O_7$ and $In_2Mn_2O_7$ differ in sign [29], it is likely that their DM constants D have opposite signs as well. Therefore, the magnon arcs of the two systems should roughly be mirror images for the same experimental setup.

Concerning transport experiments, signatures of the Weyl points are difficult to identify because magnons are bosons and all states contribute at elevated temperatures. On top of this, the Weyl points show up at a common energy; therefore, their contributions cancel each other in the integral of the transverse thermal conductivity [3,4] because they carry opposite topological charges. A mechanism which breaks the inversion symmetry allows for Weyl points with different energies; in this case, they would contribute to the transport.

Conclusion.—Ferromagnetic pyrochlores feature magnon Weyl points that can easily be tuned by an external magnetic field. Thus, the class of topologically nontrivial systems which comprises topological magnon insulators is extended to, loosely speaking, "magnon Weyl semimetals." The latter consists of breathing pyrochlores with a noncollinear ground state, reported in Ref. [14], and ferromagnetic pyrochlores that belong to a different symmetry class, as predicted in this Letter. The effect of magnon Weyl points on magnon transport of both spin and heat as well as the formation of topological interface modes [28,34] and the influence of magnon damping of topological states [35] appear worth investigating in the future.

This work is supported by SPP 1666 of Deutsche Forschungsgemeinschaft (DFG).

[1] Y. Onose, T. Ideue, H. Katsura, Y. Shiomi, N. Nagaosa, and Y. Tokura, Science **329**, 297 (2010).

[2] H. Katsura, N. Nagaosa, and P. A. Lee, Phys. Rev. Lett. **104**, 066403 (2010).
[3] R. Matsumoto and S. Murakami, Phys. Rev. B **84**, 184406 (2011).
[4] R. Matsumoto and S. Murakami, Phys. Rev. Lett. **106**, 197202 (2011).
[5] I. Dzyaloshinsky, J. Phys. Chem. Sol. **4**, 241 (1958).
[6] T. Moriya, Phys. Rev. **120**, 91 (1960).
[7] Y. Hatsugai, Phys. Rev. B **48**, 11851 (1993).
[8] Y. Hatsugai, Phys. Rev. Lett. **71**, 3697 (1993).
[9] L. Zhang, J. Ren, J.-S. Wang, and B. Li, Phys. Rev. B **87**, 144101 (2013).
[10] A. Mook, J. Henk, and I. Mertig, Phys. Rev. B **90**, 024412 (2014).
[11] H. Hasan and C. Kane, Rev. Mod. Phys. **82**, 3045 (2010).
[12] X. Wan, A. M. Turner, A. Vishwanath, and S. Y. Savrasov, Phys. Rev. B **83**, 205101 (2011).
[13] S.-Y. Xu, N. Alidoust, I. Belopolski, Z. Yuan, G. Bian, T.-R. Chang, H. Zheng, V. N. Strocov, D. S. Sanchez, G. Chang *et al.*, Nat. Phys. **11**, 748 (2015).
[14] F.-Y. Li, Y.-D. Li, Y. B. Kim, L. Balents, Y. Yu, and G. Chen, Nat. Comm. **7**, 12691 (2016).
[15] M. Elhajal, B. Canals, R. Sunyer, and C. Lacroix, Phys. Rev. B **71**, 094420 (2005).
[16] V. N. Kotov, M. Elhajal, M. E. Zhitomirsky, and F. Mila, Phys. Rev. B **72**, 014421 (2005).
[17] T. Holstein and H. Primakoff, Phys. Rev. **58**, 1098 (1940).
[18] M. V. Berry, Proc. R. Soc. A **392**, 45 (1984).
[19] J. Zak, Phys. Rev. Lett. **62**, 2747 (1989).
[20] J. H. Han and H. Lee, arXiv:1604.08290.
[21] A. A. Soluyanov, D. Gresch, Z. Wang, Q. Wu, M. Troyer, X. Dai, and B. A. Bernevig, Nature (London) **527**, 495 (2015).
[22] R. Cheng, S. Okamoto, and D. Xiao, arXiv:1606.01952 [Phys. Rev. Lett. (to be published)].
[23] S. A. Owerre, J. Phys. Condens. Matter **28**, 386001 (2016).
[24] A. A. Burkov and L. Balents, Phys. Rev. Lett. **107**, 127205 (2011).
[25] M. Hermanns, K. O'Brien, and S. Trebst, Phys. Rev. Lett. **114**, 157202 (2015).
[26] See Supplemental Material at http://link.aps.org/supplemental/10.1103/PhysRevLett.117.157204 for additional plots of the Berry curvature vector field for different directions of $\boldsymbol{n}$.
[27] J. Henk and W. Schattke, Comput. Phys. Commun. **77**, 69 (1993).
[28] A. Mook, J. Henk, and I. Mertig, Phys. Rev. B **91**, 224411 (2015).
[29] T. Ideue, Y. Onose, H. Katsura, Y. Shiomi, S. Ishiwata, N. Nagaosa, and Y. Tokura, Phys. Rev. B **85**, 134411 (2012).
[30] M. Mena, R. S. Perry, T. G. Perring, M. D. Le, S. Guerrero, M. Storni, D. T. Adroja, C. Rüegg, and D. F. McMorrow, Phys. Rev. Lett. **113**, 047202 (2014).
[31] K. Riedl, D. Guterding, H. O. Jeschke, M. J. P. Gingras, and R. Valenti, Phys. Rev. B **94**, 014410 (2016).
[32] H. J. Xiang, E. J. Kan, M. H. Whangbo, C. Lee, S.-H. Wei, and X. G. Gong, Phys. Rev. B **83**, 174402 (2011).
[33] K. Zakeri, Y. Zhang, and J. Kirschner, J. Electron Spectroscopy Related Phenomena **189**, 157 (2013).
[34] A. Mook, J. Henk, and I. Mertig, Phys. Rev. B **91**, 174409 (2015).
[35] A. L. Chernyshev and P. A. Maksimov, arXiv:1606.09249.